Accepted Manuscript

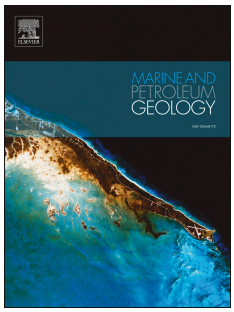

Methane-derived authigenic carbonates on accretionary ridges: Miocene case studies in the northern Apennines (Italy) compared with modern submarine counterparts

C. Argentino, S. Conti, G. Crutchley, C. Fioroni, D. Fontana, J.E. Johnson

PII: S0264-8172(19)30018-2

DOI: https://doi.org/10.1016/j.marpetgeo.2019.01.026

Reference: JMPG 3695

To appear in: *Marine and Petroleum Geology*

Received Date: 19 September 2018

Revised Date: 18 January 2019

Accepted Date: 18 January 2019

Please cite this article as: Argentino, C., Conti, S., Crutchley, G., Fioroni, C., Fontana, D., Johnson, J.E., Methane-derived authigenic carbonates on accretionary ridges: Miocene case studies in the northern Apennines (Italy) compared with modern submarine counterparts, *Marine and Petroleum Geology* (2019), doi: https://doi.org/10.1016/j.marpetgeo.2019.01.026.

Methane-derived authigenic carbonates on accretionary ridges: Miocene case studies in the northern Apennines (Italy) compared with modern submarine counterparts

Argentino C.[a*], Conti S.[a], Crutchley G.[b], Fioroni C.[a], Fontana D.[a], Johnson J.E.[c]

[a] Department of Chemical and Geological Sciences, University of Modena and Reggio Emilia, Modena, Italy.

[b] GNS Science, Lower Hutt, New Zealand.

[c] Department of Earth Sciences, University of New Hampshire, Durham, New Hampshire, USA

Abstract

We present new field data from three outcrops of Miocene methane-derived authigenic carbonates in the foredeep of the northern Apennines that contain chemosynthetic fauna and record a long history (~ 1 Ma) of shallow fluid seepage linked to seafloor anaerobic oxidation of methane. The studied outcrops show similar features in terms of carbonate morphology, facies, spatial distribution and lateral and vertical contacts with the enclosing sediments. Methane-derived carbonates occur in two structural positions: 1) on the slope of the accretionary wedge in hemipelagites draping buried thrust-related anticlines, and 2) at the leading edge of the deformation front in the inner foredeep, within fault-related anticlines standing above the adjacent deep seafloor as intrabasinal ridges. We compare fossil seeps with two extensively investigated modern analogues: the Hikurangi Margin, offshore New Zealand and Hydrate Ridge, on the Cascadia margin, offshore the U.S.A. These analogues share a similar compressive structural setting and are marked by the presence of variably extensive and voluminous methane-derived carbonate bodies and chemosynthetic fauna on the present-day seafloor. The comparison allows us to propose a model for the evolution of fluid seeps on thrust-related ridges. At the deformation front, uplift and geometry of the anticlinal ridges are

controlled by the growth of splay faults, mostly blind, connected to the basal detachment, favoring the migration of fluids toward the incipient anticline. Fold development generates extensional stresses in the hinge zone of the anticline, promoting the development of normal faults; fluid migration pathways and seafloor seeps shift from the forelimb toward the crest of the ridge as the structures evolve. After reaching a mature stage within the wedge, the structure is less active and buried in the slope environment of the evolved prism In the slope setting, far from the deformation front, thrust faults and extensional faults in buried anticlines remain the main fluid migration pathways to sustain seepage at the seafloor.

Key words: Methane-derived carbonates, accretionary prism, anticlinal ridge, fluid migration, Miocene seep, northern Apennines, Hydrate Ridge, Hikurangi slope.

1. Introduction

Expulsion of hydrocarbon-rich fluids is a common process in accretionary wedges where tectonic thickening and underplating generate pore-fluid overpressures and induce fluid migration (Gill et al., 2005; Ding et al., 2010; Crutchley et al., 2015; Klaucke et al., 2015; Tavani et al., 2015). Thrust-related anticlines on the lower slope of accretionary wedges and in the inner foredeep represent ideal structures for the accumulation, trapping and dissipation of methane-rich fluids (Moretti et al., 2002; Morley, 2007; Barnes et al., 2010; Leifer et al., 2010; Netzeband et al., 2010; Evans and Fischer, 2012; Morley et al., 2014; Fraser et al., 2016), and may create the optimal conditions for gas hydrate formation and destabilization (Judd and Hovland, 2009; Laird and Morley, 2011; Krabbenoeft et al., 2013).

In foredeep settings in front of accretionary prisms, large amounts of organic matter of terrestrial and marine origin accumulate within turbidite-rich hemipelagic sediments (Canfield,

1994). During burial, the organic matter undergoes several biogeochemical processes that lead to its progressive mineralisation (eg. Jørgensen, 1982; Canfield, 1994). The organic matter that escapes oxidation close to the seafloor is converted to methane by microbial processes involving methanogenic archaea in the upper sedimentary column and by thermal maturation at greater depths. Methane-rich fluids formed at depth tend to migrate upward through diffuse intergranular flow and/or advective flow through structural or stratigraphic permeable pathways (e.g. Moore et al., 1990; Carson and Screaton, 1998; Krabbenoeft et al., 2013), eventually mixing with shallow methane sources. Thrust-related anticlines can provide local extensional settings at their crests for methane-rich fluid expulsion (eg. Morley, 2007; Leifer et al., 2010; Laird and Morley, 2011; Evans and Fischer, 2012; Beaudoin et al., 2015), favouring the precipitation of thick authigenic carbonates (Teichert et al., 2003; Johnson et al., 2003, 2006; Greinert et al., 2010) linked to the anaerobic oxidation of methane (AOM). Methane that is not consumed via AOM, either advectively escapes to the seafloor resulting in methane seepage, or remains trapped below the AOM zone where it can accumulate as free gas or gas hydrate, if within the gas hydrate stability zone.

The contribution of deep fluid sources to the shallow pore-water methane budget increases with distance from the toe of the accretionary prism (Torres et al., 2004), reflecting upward advection in response to burial and tectonic compression that increases pore pressure at depth during continued deformation of the wedge. Deep fluids may also flow along the basal décollement and reach the seafloor through frontal thrusts, at the deformation front (Yamada et al., 2014; Chen et al., 2017). The concomitance of tectonic activity, topographic relief and escape of methane may contribute to generate soft sediment deformation and sedimentary instability (Cochonat et al., 2002; Johnson et al., 2006; Conti et al., 2008, 2010; Ellis et al., 2010).

The northern Apennine orogenic belt consists of an uplifted paleo-accretionary prism that was mainly formed during the Neogene and is associated with carbonates recording seepage activity (Conti et al., 2004; Dela Pierre et al., 2010). Recent studies on Miocene seepage in the northern Apennines have demonstrated that seep-carbonates formed at the front of the paleo-wedge (Conti et

al., 2017 and references therein) during different stages of foredeep migration, recorded as synsedimentary growth strata on thrust-related anticlines. Such examples provide a unique opportunity to better constrain relationships among anticlinal growth, fluid expulsion and carbonate precipitation. In this study we present new field data from three key outcrops in the northern Apennines, representative of a long and dynamic history of seepage (~ 1 My) during the advance of the Miocene wedge-foredeep system. Stratigraphic and structural results from our field study are compared with two extensively investigated modern analogues that share a similar structural setting near the fronts of accretionary prisms: the Hikurangi Margin, offshore New Zealand's east coast, and at Hydrate Ridge, in the Cascadia accretionary wedge offshore Oregon, U.S.A. These modern methane-related seep systems are marked by the presence of thick MDAC bodies on the seafloor (Bohrmann et al., 1998; Trehu et al., 1999; Greinert et al., 2001; Johnson et al., 2003; Klaucke et al., 2010; Krabbenhoeft et al., 2013). It has been noted that modern analogues reveal only partial stages of seepage activity (e.g. Plaza-Faverola et al., 2011; Crutchley et al., 2015; Klaucke et al., 2015; Mohammedyasin et al., 2016) while the identification of buried authigenic carbonates may be difficult on seismic data due to resolution limits (Andresen, 2012; Ho et al., 2012). On the other hand, seismic and seafloor data from modern analogues allow observations at a basin-wide scale and may allow the recognition of fluid migration pathways that are rarely identified in the geological record (Nyman et al., 2010; Nelson et al., 2017).

The objective of this study is to improve our understanding of methane-related seepage systems on accretionary settings, by integrating structural and stratigraphic evidence from onshore outcrop data with modern offshore analogues. We first present a summary of recurring features at three key seep carbonate outcrops in the northern Apennines, in terms of structural position, geometry and bounding relationships. We then compare these to lower resolution information from modern analogues on the Hikurangi and Cascadia margins. This comparison allows us to propose an evolutionary model of paleo-seepage on fault-related ridges in accretionary settings, and provides new insights into the variability and dynamics of ancient and modern seep-carbonate settings.

2. Geological setting

2.1 Apennine structural setting

The northern Apennine mountain chain is a fold and thrust belt characterized by the stacking of multiple structural units of oceanic and continental origin (Fig. 1). The complex structure of the chain is a result of convergence and collision between the European and the Adria plates from the Mesozoic to the present. Starting from the Early Cretaceous, an intraoceanic accretionary prism caused the progressive consumption of the Piedmont-Ligurian Ocean, a portion of the Tethys Ocean (Argnani and Ricci Lucchi, 2001). Closure of the ocean during Middle-Late Eocene caused rapid uplift and erosion of the Alpine orogenic wedge and the inception of continental collision. During the collision (late Oligocene to Recent) the internal oceanic units (Ligurian units) were placed over the western continental margin of Adria (Tuscan and Umbro-Romagna units) (Fig. 1). Subduction of the Adria plate under the European lithosphere brought about flexure of the foreland and the formation of foredeep basins. The migration of the tectonic front is generally related to roll-back of the subducting Adriatic slab (Carminati and Doglioni, 2012). Migration was accompanied by the development of small basins on top of the orogenic wedge, filled by Epiligurian units (Conti et al., 2016; Argentino et al., 2017) (Fig. 1). Beyond the advancing Apenninic front, foredeep basins were mainly filled by sheet-like turbidites within depocenters that migrated to the northeast and were progressively incorporated into the prism (Fig. 2).

The advance of the accretionary wedge caused the foredeep to segment into inner and outer sectors. Successive stages of migration, uplift and closure produced numerous lithostratigraphic units with complex lateral relationships (Tinterri and Muzzi-Maghalaes, 2011; Di Giulio et al., 2013). A simplified scheme of the units filling the foredeep basins during the Miocene is presented in Figures 1 and 2. The age of the Apennine thrust belts decreases toward the northeast, in the

direction of wedge advancement and foredeep migration (Fig. 1). In the Burdigalian, closure of the Tuscan foredeep (filled by turbidites of the Falterona Fm) was followed by deposition of slope hemipelagites of the Vicchio Fm (Figs. 1, 3) (Conti et al., 2010, 2017). During the Langhian, the newly formed foredeep was filled by thick turbidites of the Marnoso-arenacea Fm (Umbro-Marchean units); its progressive involvement in the accretionary wedge resulted in the fragmentations of the inner sector through the development of intrabasinal highs draped by hemipelagites (Pelitic lithofacies of Fig. 3). These fine-grained sediments on top of the structural highs host several large seep-carbonate bodies, which are the subject of the present study.

2.2 Authigenic carbonates - isotopic evidence of methane seepage

The carbon isotopic composition of authigenic carbonates can be used to assess their origin from methane via either AOM, organoclastic sulfate reduction, or methanogenesis (e.g. Teichert et al., 2014). The $\delta^{13}C$ composition of the biogenic methane is significantly depleted in ^{13}C (values as negative as -110‰ VPDB) compared to thermogenic methane (-50 to -30‰ VPDB) (Whiticar, 1999). However $\delta^{13}C$ values recorded by MDAC at seeps are generally heavier than methane carbon due to mixing with dissolved inorganic carbon from sea-water (-3‰) and from mineralisation of marine organic matter (-25‰ to -20‰) (Whiticar, 1999). Typical MDAC $\delta^{13}C$ values range from -60‰ to -30‰ (Judd and Hovland, 2009). Seep-impacted sediments are characterized by high concentrations of reduced compounds (H_2S, CH_4) which diffuse from the sulfate-methane transition (SMT) and may reach the seafloor and sustain characteristic chemosynthetic ecosystems including bacterial mats and a variety of clams, mussels and tubeworms (e.g. Kiel and Tyler, 2010; Boetius and Wenzhöfer, 2013; Taviani, 2014; Grillenzoni et al., 2017). In the northern Apennines, several previous studies have shown that the stable isotope (C and O) compositions of carbonates and chemosynthetic fauna allow the identification as MDACs (Conti et al., 2004, 2017; Argentino et al., 2017). Table 1 summarises results for the outcrops examined in

this study: authigenic micrite ranges from -42‰ to -25‰ and calcite cements from -30‰ to -14‰. Enriched $\delta^{13}C$ values suggest some influence of organoclastic sulfate reduction and/or biogenic fossil influence in these locations. In Table 1 the carbonate mineralogy is also reported. From previously published XRD analyses (Conti et al., 2004) we observe a dominance of low-magnesium calcite with minor high-Mg calcite and dolomite. The presence of chemosynthetic fauna in our outcrops is consistent with a surface or shallow subseafloor environment that may have been episodically charged with methane through time.

3. Methods

Three outcrops (Moggiona, Corella, Castagno d'Andrea; Figs. 1, 3) were selected for their good stratigraphic exposure and wide lateral (up to 600 m) and vertical (50 m) extent. Carbonate bodies are concordant within vertically to sub-horizontally bedded host rocks, facilitating outcrop observations of their lateral geometries, thicknesses and internal facies. A detailed geological investigation was performed at each site and was focused on the assessment of carbonate body geometries, terminations and contacts with the host sediments, spatial distribution and relationships with nearby regional structures. These field observations were integrated with published studies (Conti et al., 2004, 2010; Fontana et al., 2013) in order to provide a reliable scheme representative of the outcrop-scale variability of seep-impacted deposits of the Apenninic foredeep. In our study we also consider small scale recurring features such as the presence of minor carbonate blocks around the main bodies and facies distribution, as they help our understanding of the physical evolution of the seepage (e.g. growth directions, seepage intensity). The age of the main authigenic carbonate bodies was determined based on biostratigraphic analysis of nannofossils in samples of the over- and underlying host sediments.

4. Results from Miocene case studies in the Apennines

In this section we present a description of the outcrops, their structural setting and an estimate of seepage duration. A summary of recurring features at these seep carbonate outcrops in terms of morphology, spatial distribution, lateral and vertical contacts with enclosing sediments and carbonate facies is reported in Table 2.

4.1 Field observations of carbonate outcrops

Moggiona [43°47'02.6"N 11°46'58.1"E]

Outcrop description. MDACs are present in the basal member of Vicchio Fm. (Fig. 3a) representing the early stage of the closure of the Outer Tuscan foredeep (Falterona Fm.). The base of the member is not exposed, as it is cut by the regional overthrust of the Falterona Fm. The basal Vicchio member is characterized by marls and silty marls; the silt content increases upward as well as that of sporadic cm-thick layers of fine-grained arenites. MDACs are located in the footwall syncline at the base of the thrust, close to the tectonic lineament (Fig. 3a). The thickness of the MDAC interval is 20-30 m with a lateral extent of ~200 m. Bedding attitude is vertical-subvertical, with an average strike N70W.

Carbonate morphology and contacts with enclosing sediments. MDACs form bodies ranging from 5-100 m and up to 8 m thick (Figs. 5a, b); two smaller meter-sized blocks are also present. The carbonate bodies have a vertical attitude and are concordant to host sediments; they strike parallel to the main Apennine structural trends. Morphologies are mostly stratiform although the main carbonate body presents an irregular profile with strong lateral thickness variations. The contact between carbonates and host sediments varies from sharp to gradual in correspondence with progressively decreasing cementation. Several different types of contacts can be recognized: pinch-out lateral terminations, bifurcations, multiple interdigitation of carbonates with enclosing marls, lateral repetitions of rounded concretions and nodules (Fig. 5c).

Facies association. The basal portion of large carbonate bodies is characterized by dense arrays of conduits with orientations varying from vertical to sub-horizontal, frequently displaying crosscutting relationships (Figs. 5b, 6a). Conduits are generally a few centimeters in diameter, with circular cross sections and few decimetre long; infillings of silty particles typically associated with coquina debris. Conduit-rich facies give way to mottled micrites pervaded by a dense network of thin (mm) fractures that locally widen into drusy-like cavities. The top of the carbonate bodies is commonly marked by assemblages of chemosynthetic fauna, either articulated and in life position or dismembered shells oriented parallel to bedding.

Age. Based on nannofossil assemblages of the enclosing marls, the age of the seep carbonates can be ascribed to the Burdigalian, MNN3b biozone (Conti et al., 2017) (Fig. 4).

Castagno d'Andrea [43°53'15.1"N 11°40'32.6"E]

Outcrop description. The outcrop exposes in the basal portion of a pelitic interval made up of marls and silty marls within the Marnoso-arenacea Fm. The maximum thickness of the pelitic interval is ~200 m and extends laterally over ~12 km. The outcrop is within a gentle synclinal structure dipping at N30E (Fig. 3b). The southern part of the interval is not exposed due to the regional thrust of the outer Tuscan units over the Marnoso-arenacea Fm., detached at the level of varicoloured marls and mudstones (Fig. 3b). The outcrop includes four large seep-carbonate bodies, vertically staked and distributed on 3 stratigraphic horizons concordant to the enclosing sediments and to main structural trends (Fig. 3b). Large carbonate bodies are laterally surrounded by small bodies concordant to enclosing strata (Fig. 7). Sediment instability features, in the form of small-scale slumps, occur locally in host sediments above the carbonate bodies (Fig. 3b).

Carbonate morphology and contacts with enclosing sediments. Carbonates display different morphologies (pinnacle-like to stratiform), from 12-30 m wide and 5-10 m thick (Fig. 7). The middle and upper stratiform bodies are connected both by pinnacular structures (up to 8 m high) with an irregular profile laterally interfingering with host pelites, and by branching structures (Figs.

7a, b, c). The basal contact is highly irregular marked by < 0.5 m sized micritic concretions (Fig. 7d). Lenticular bodies have an irregular thickness (Fig. 7a). Lateral transitions to enclosing sediments are sharp to gradual, with lateral repetitions of small concretions.

Facies association- Stratiform bodies are characterized by an irregular framework of fractures and drusy-like cavities, associated with branched veins; in the upper portions, dense arrangements of lucinid-like clams are observed. The main facies in pinnacle-like bodies are polygenic breccias with mixing of various lithotypes and disarticulated clams (Fig.7c). Clasts are derived from older underlying successions and from previously precipitated carbonate crusts. Monogenic breccias caused by autoclastic processes are present in all bodies (Fig. 6b).

Age. Calcareous nannofossils of the enclosing marls indicate the Langhian MNN5a subzone (Conti et al., 2004) (Fig. 4).

Corella [43°56'59"N 11°34'59.8"E]

Outcrop description. The outcrop is located within the same pelitic interval as Castagno d'Andrea, approximately 10 km northwest, in a higher stratigraphic position, close to the top of the interval (Fig. 3c). The study area is within an anticlinal structure whose axis is oriented NW-SE, parallel to the thrust of the Outer Tuscan Units over the Marnoso-arenacea Fm. (Figs. 1, 3c). Carbonates are located on the northern flank of the anticline and show vertical attitudes as the surrounding strata and to the main structural trends. Six large carbonate bodies and several minor meter-sized blocks are vertically distributed within two stratigraphic horizons (Fig. 8a).

Carbonate morphology and contact with enclosing sediments- Carbonates are stratiform to lenticular, with a lateral extent between 50-230 m and thicknesses up to 30 m (Fig. 8b). Basal and upper surfaces are rather flat. Lateral contacts are usually sharp, with pinch-out terminations (Figs. 8a, b); in a few cases the contact is marked by bifurcations giving way to smaller (<1 m) blocks. Larger carbonate bodies are vertically connected by irregular minor meter-sized bodies, or by highly cemented strata (Fig. 8c).

Facies associations. The basal portion of bodies is characterized by an irregular framework of fractures, conduits (Fig. 6c) and drusy-like cavities and polygenic breccias (mm to cm sized) associated with disarticulated bivalves (Fig. 8b). Monogenic breccias occur at various levels. A dense concentration of articulated lucinid-like bivalves is observed at the top of the bodies (Fig. 6d). Structures indicating small-scale sedimentary instabilities are scattered throughout (Fig. 3c).

Age. The nannofossil assemblages of the pelitic interval are characterized by *Sphenolithus heteromorphus* associated with specimens of *Helicosphaera waltrans*, and the concurrent absence of *Helicosphaera walbersdorfensis* and *Helicosphaera ampliaperta*. Despite the moderate state of preservation and the scarce abundance of nannofossils, the interval can be confidently ascribed to the Langhian MNN5a subzone (Fig. 4).

4.2 Structural position of seep carbonates

The three outcrops reported above are representative of the regional development of MDAC in two main structural positions within the Apenninic accretionary system: internal to the prism, within buried fault-related anticlines along the outer slope close to the orogenic front; and in an external position in the inner foredeep, in fault-related anticlines that form intrabasinal ridges with seafloor expression.

(1) Internal position: Moggiona is representative of this setting (Fig. 2). MDACs in this setting are hosted in fine-grained sediments draping thrust-bounded folds and buried ridges constituted by the older accreted turbiditic units. Thrust faults are mostly blind and only in few cases reach the surface. Slope sediments with MDAC occurrences cover a wide extent, up to 100 km parallel to the structural trend of the chain, and record the closure stage of the foredeep before overriding by allochtonous units. Buried structures have been reactivated generating small ponded basins that were successively incorporated in the orogenic wedge.

(2) External position in the inner foredeep: Castagno d'Andrea and Corella are representative of this setting (Fig. 2). Seep-carbonates are hosted in fine-grained intervals sedimented above these intrabasinal ridges surrounded by basinal turbidites. The ridges form topographic highs that extend laterally for 10-15 km. In this setting, thrust faults are connected to the basal detachment through growing splay faults. After having reached a mature stage, the structure was deactivated and accreted in to the prism. Castagno d'Andrea and Corella are developed in the same intrabasinal high, and represent two subsequent phases of seepage related to growth of the structure.

4.3 Estimated duration of seepage activity

Our structural and stratigraphic mapping and the presence of MDAC and chemosynthetic fauna above growing anticlinal structures suggest these carbonates are likely associated with paleo-methane seepage during the Miocene. The duration of seepage activity, however, is difficult to assess from the fossil record. An estimate can be obtained from the age of marly sediments enclosing the MDAC, dated using nannofossil stratigraphy. However, this method is limited by the uncertain relationships between the rates of sedimentation of the marls and those of carbonate precipitation. Our observations of chemosynthetic fauna within the MDAC are consistent with near seafloor precipitation and seepage concomitant with sedimentation. If so, the bracketing ages from nannofossil biostratigraphy provide a maximum duration of seepage activity. A complementary approach for constraining the lifespan of the seepage system is based on the average growth rate of seep carbonates, as reported in the literature. Bayon et al. (2009) measured the U/Th ages of a carbonate crust (6 cm thick) at the Central Nile deep-sea fan and estimated the average aragonite and high-Mg calcite growth rates, as 5 cm/ka and 0.8 cm/ka, respectively. Luff and Wallmann (2003) obtained a similar growth rate for authigenic calcite based on a numerical model (precipitation of 1-2 cm of calcite in 310 years). Applying these values for calcite growth to the Corella outcrop, the thicker carbonate body (~30 m; Fig. 3C) would record minimum period of ~

600 ka, while minor bodies (~10 m thick) could have formed in ~200 ka. These minimum values are within the estimated maximum duration of the nannofossil biozone of the host sediments (MNN5a, ~ 1 Ma). These values should be considered a rough estimate, since carbonate growth directions may vary in response to fluids pathways around the growing authigenic body (Hovland, 2002) and fluid flow can vary significantly over time, with episodes of high flux giving way to periods of low intensity and minor carbonate precipitation (Teichert et al., 2003). Carbonate precipitation and seepage activity in structurally-controlled systems is also sensitive to fault-valve behavior (Bolton et al., 1999; Sibson, 2000; Teichert et al., 2003). Despite these limitations, the values estimated for the duration of seepage on thrust-related anticlines of the Miocene foredeep system, are on the order of several hundred thousand years. This estimate is in agreement with data obtained from Montepetra intrabasinal high, late Miocene (Conti et al. 2010).

5. Modern seep sites and methane-derived carbonates at accretionary wedges

We present information from two present-day settings of gas seepage and carbonate formation, the Hikurangi and Cascadia convergent margins. Seepage systems have been investigated using geophysical methods (multibeam bathymetry and backscatter imagery, seismic reflection profiles of varying frequency content) that provide information over large areas and at variable subsurface resolution (10^{-1}- 10^{1} m), complemented by investigations of individual seeps using seafloor observations and sampling.

5.1 Hikurangi Margin, offshore New Zealand

Methane seepage resulting in the development of authigenic carbonates is widespread on New Zealand's Hikurangi subduction margin (Greinert et al., 2010), where oblique convergence between the two colliding plates causes pronounced folding, faulting and pore fluid expulsion

(Townend, 1997). Studies of pore fluid chemistry at particular seep sites indicate a biogenic source for the methane being released (e.g. Koch et al., 2016), but there are also indications of deeply-rooted fluid sources migrating upward along thrust faults to the seafloor (e.g. Plaza-Faverola et al., 2016). As such, a thermogenic origin for gas at some seep sites cannot be ruled out. Of the sites published to date on the margin most are observed to occur on the crests of thrust-faulted anticlinal folds along the mid slope of the deforming wedge (Barnes et al., 2010; Greinert et al., 2010). This correlation indicates preferential fluid flow focused through thrust-fold structures, as opposed to the intervening slope basins, where strata are more flat lying and deep-seated thrust faults do not occur. Several studies on the Hikurangi margin have shown various seep carbonates on the ridges, recognized as highly-reflective areas of seafloor of anomalous topographic relief (Jones et al., 2010; Liebetrau et al., 2010; Dumke et al., 2014; Koch et al., 2015; Plaza-Faverola et al., 2016), some of which cover areas several hundreds of meters across. On Opouawe Bank (near the southern end of the margin), high-resolution seismic profiles allowed the recognition of strong positive amplitude reflections closely distributed above and adjacent to seismic chimneys which may indicate the presence of carbonates and/or gas hydrates (Krabbenhoeft et al., 2013; Koch et al., 2015). In the Wairarapa Area, Klaucke et al. (2010) observed several blocks of authigenic carbonates up to 25 m in diameter, a few meters high at the seafloor, which form clusters surrounded by small satellite blocks. At the Tui and North Tower seep sites, carbonates form massive chemoherms that stand several meters above the seafloor (Bowden et al., 2013); in the subsurface they intercalate laterally with well-stratified turbidites and may have dimensions exceeding the area of high reflectivity mapped at the seafloor. Other examples from the Omakere Ridge show elevated features several meters high, with various shapes from oval or horse-shoe like to ridge-like features. Jones et al. (2010) reported a knoll up to 12 m high and ~400 m in diameter at Bear's Paw site. The distribution of chemosynthetic communities and seep carbonates on the Hikurangi Margin is variable and ranges from seeps with no-MDACs and no-chemosynthetic fauna to those with occurrences of massive carbonates with large areas of *Calyptogena* sp. shells, or tubeworms (Bowden et al., 2013).

364

365 *5.2 Seeps at Hydrate Ridge, Cascadia Margin, Oregon U.S.A.*

366

367 The formation and continued evolution of the Cascadia accretionary wedge is a result of the
368 oblique subduction of the Juan de Fuca and Gorda plates beneath the North American plate offshore
369 western North America. Abyssal plain sediments are dominated by turbidites and hemipelagites of
370 the Astoria and Nitinat submarine fans are accreted and uplifted into a series of thrust ridges and
371 intervening slope basins that form the active accretionary wedge. The structures of the Cascadia
372 accretionary wedge were initially identified and mapped using seismic reflection data and high-
373 resolution bathymetry by Goldfinger et al. (1992, 1997) and MacKay et al. (1992). Sediment
374 deformation is concentrated at the leading edge of the deformation front, where material is folded
375 and faulted into elongate anticlinal ridges that stand as much as 700 m above the adjacent abyssal
376 sea floor, thus representing intrabasinal highs. Individual ridges are typically 20-30 km in length, a
377 few kilometers in width, and in many cases arcuate in plan view (Davis and Hyndman, 1989; Tryon
378 and Brown, 2001). The structures generally strike parallel to the main structural trends, plunging
379 laterally towards their closure. Hydrate Ridge is the second anticlinal ridge back from the
380 deformation front of the Cascadia accretionary wedge and is formed from both seaward and
381 landward vergent thrust faults (Johnson et al., 2006). Two of nine margin-wide, left-lateral strike-
382 slip faults (Goldfinger et al., 1997) bound Hydrate Ridge to the north and south. The presence of
383 mixed vergence thrusts, overlying thrust-fold ridges and slope basins, and strike-slip faults within
384 the Hydrate Ridge region has resulted in deformation to create high permeability dipping
385 stratigraphic horizons and fractures (Torres et al., 2004) that facilitate tectonic dewatering (Johnson
386 et al., 2003; 2006).

387 The crest of Hydrate Ridge is associated with an abundance of authigenic carbonates (slabs,
388 crusts, buildups), gas hydrates and seafloor methane seeps (Suess et al., 1999; Trehu et al., 1999;
389 Greinert et al., 2001; Johnson et al., 2003; Torres et al., 2004). These features are inferred to reflect

up-dip migration pathways driven by anticlinal focusing of fluids (Johnson et al., 2003; Weinberger et al., 2005). Hydrate Ridge hosts remarkable seep-carbonate complexes, forming pinnacles up to 90 m high and 150 m wide (Bohrmann et al., 1998; Greinert et al., 2001; Teichert et al, 2003). Chemosynthetic fauna (e.g. Suess et al., 1999) associated with seep-carbonates are observed on the crest of Hydrate Ridge and have been mapped by sidescan sonar (Johnson et al., 2003). Drilling during ODP Leg 204 recovered abundant gas hydrate, free gas, authigenic carbonates, and AOM related diagenetic products within the summit of southern Hydrate Ridge and identified the importance of both structural and stratigraphic conduits for methane charged fluid flow toward the crest of the structure (Trehu et al., 1999; Torres et al., 2004).

6. Discussion: the Miocene seeps compared with modern analogues.

The features observed within outcrops of Miocene methane-derived authigenic carbonates (Table 2) show several similarities with active seepage systems on accretionary ridges, in terms of structural position, dimension and geometry of the authigenic bodies, and their spatial distribution. Below we first compare the Apennine seeps within the prism to those of the Hikurangi margin, then the seeps of the inner foredeep intrabasinal highs to those of the Cascadia margin. Finally, we present a model of the evolution of seepage systems on accretionary margins.

6.1 *Seeps on the slopes of the accretionary wedges: comparison with the Hikurangi margin*

The modern wedge-slope seeps of the Hikurangi margin of New Zealand are comparable with the Moggiona seeps of the Apennines in terms of structural position, morphology and spatial distribution of the carbonate deposits. In both cases, seep-carbonates precipitated on the slope of the accretionary wedge mainly within hemipelagites draping thrust-bounded folds that are composed of the older imbricated units. Deep-rooted thrust faults are assumed to have acted as the primary

pathways for the upward migration of methane-rich fluids. In Hikurangi slope, closer to the seafloor, extensional faulting around the apex of flexural folds (e.g. Barnes et al., 2010; Riedel et al., 2018) provides permeable pathways for fluid ascent. In the final stages of ascent to the seafloor, where confining pressures reduce even further, gas can form its own migration pathways that do not depend on pre-existing structural fabrics (Koch et al., 2015; Riedel et al., 2018). It is in this sub-seafloor depth interval (10s of meters) that we expect free gas migration to diverge into multiple ascent pathways, rather than being confined to particular structural conduits. This process could be manifested in patches of authigenic carbonate precipitation with no preferential spatial pattern. On the other hand, some carbonate distribution patterns on the Hikurangi margin are clearly related to inherent tectonic structures (e.g. at Omakere Ridge). In this case, it is clear that fluid flow through these structures controls the overall distribution of seepage and carbonate precipitation at the seafloor, which follow structural trends. This situation is well expressed by the Moggiona outcrop (Fig. 9a) and it has also been described by Conti et al. (2010) for the Upper Miocene Montepetra seep (northern Apennines), developed in a similar context. The seep-impacted deposits and their host structures were eventually incorporated into the orogenic wedge and fluid migration was deactivated, but the geologic record of seepage processes remain preserved. The Moggiona seep-carbonates and the modern seeps at Hikurangi Margin also share similarities in terms of faunal content and the geometries and of the carbonate bodies. Both form wide stratiform bodies with complex lateral terminations and multiple lateral alternations with enclosing pelitic sediments. The spatial distribution of satellite blocks at the Moggiona outcrop is similar to the carbonate blocks that have been observed at the Omakere Ridge (Liebetrau et al., 2010; Bowden et al., 2013).

6.2 *Seeps on intrabasinal highs: the comparison with Hydrate Ridge*

Apennine seeps in the inner foredeep show several structural and stratigraphic similarities with those observed on Hydrate Ridge. The structural position and lateral extent of the fossil pelitic

interval hosting carbonates (~12km) is comparable in scale to that of the anticlinal ridges of the Cascadia Margin (Davis and Hyndman, 1989, Tryon et al., 2001). At Hydrate Ridge, tectonic deformation and accretion of thick saturated turbidites promoted enhanced dewatering and fluid migration along the basal detachment and through splay faults. Permeable stratigraphic layers within the hangingwall and footwall sequences of thrust faults may act as secondary pathways that focus fluid flows towards ridge crests (MacKay et al., 1992). Extensional faults and fractures develop at the crest of the intrabasinal high as a response to flexural extension of the thrust-related folds and/or hydrofracturing related to excessive pore pressures (e.g. Trehu et al., 2004; Crutchley et al., 2013). Additional similarities between the Miocene seeps on thrust-related anticlines and the modern seeps of Hydrate Ridge include carbonate morphology and facies. The Castagno d'Andrea seep-carbonates form pinnacular-like geometries comparable to those reported from Hydrate Ridge, although at a smaller scale. Detailed facies analysis of the fossil seeps revealed the presence of intraformational breccias, hydrofractures and lucinid-rich facies (Figs. 6) similar to facies reported at Hydrate Ridge by Greinert et al. (2001). In some cases the Miocene carbonates include vuggy facies that strongly suggest a carbonate-forming mechanism by growing and decomposing gas hydrates (e.g. Bohrmann et al., 1998). The contribution of paleo-gas hydrate destabilization to the precipitation of authigenic carbonates in the northern Apennines has been hypothesized by Conti et al., (2010) based on heavy oxygen isotope signatures and the presence of clathrite-like carbonate facies (breccias, pervasive non-systematic fractures, vuggy fabrics). These proxies have not been observed in the outcrops presented in this study. However, the assessment of paleo-gas hydrate occurrence and destabilization is challenging and high-spatial resolution techniques and *in situ* measurements as reported by Bojanowski et al. (2015) could provide more robust evidence. Paleobathymetric estimates of Miocene seep-carbonates based on plankton/benthos ratio in host sediments (Aharon and Sen Gupta, 1994; Grillenzoni et al., 2017), place the Apennine seepage systems at the upper-middle bathyal zones (~1000 m depth), likely within the gas hydrate stability zone. A similar depth for gas hydrate occurrence in the Oligocene-Miocene is postulated by Pierre

and Rouchy (2004) for the western Mediterranean, by Bojanowski (2007) for the Silesian Basin and by Dela Pierre et al. (2010) for the Tertiary Piedmont basin. The hypothesis of paleo-gas hydrate occurrence in the Apennine ridge is also supported by the frequent association of seep-carbonates with small-scale sedimentary instabilities within the same pelitic interval and in close proximity (Conti et al., 2008, 2010), which is a common condition also at modern counterparts (e.g. Cochonat et al., 2002; Johnson et al., 2006; Ding et al., 2010; Ellis et al., 2010; Klaucke et al., 2015).

6.3 A model of seepage evolution on accretionary ridges

The comparison of fossil seeps with modern counterparts allows us to propose an evolutionary model of the Apennine seeps, consistent with reconstructions reported for modern analogues (Fig. 9). Our results support a link between the development of thrust-related anticlines and the onset and evolution of seepage along the wedge-foredeep system as a whole. In particular, based on the distribution, morphology and stratigraphic position of seep carbonates, we assume that seepage occurs in specific positions controlled by the hosting thrust-fold structure.

In the inner foredeep, at the leading edge of the deformation front, blind faults connected to the basal detachment produce broad anticlines. During this early stage of development of an anticlinal ridge, migrating fluids are conveyed toward the incipient anticline and seepage is expected to occur at the forelimb in correspondence with the propagation of the thrust fault to the seafloor (Fig. 9b1), consistent with the model of Klaucke et al (2015). The Castagno d'Andrea outcrop is representative of this early stage of seepage, with seep carbonates are stratigraphically located at the base of the pelitic interval, close to the thrust fault (Fig. 3b). The occurrence of several vertically stacked carbonate bodies of moderate thicknesses testifies to the intermittent nature of seepage activity. As deformation proceeds, fault-related folding causes the progressive growth of the ridge. Seepage is inferred to move toward the hinge zone of the anticline, as extensional stresses create well-developed fault-fracture systems that provide efficient pathways for migrating fluids at the crest

(Fig. 9b), as has been observed at modern sites worldwide (Johnson et al. 2003; Morley, 2007; Barnes et al. 2010; Crutchley et al 2010, 2013; Leifer et al., 2010; Laird and Morley, 2011; Evans and Fischer, 2012; Krabbenhoeft et al. 2013; Morley et al., 2014; Beaudoin et al., 2015). During this mature stage, the flux of methane-rich fluids is more stable and vigorous at the crest of the ridge, promoting the precipitation of thick authigenic carbonates near the seafloor that record prolonged seepage activity. We interpret the Corella outcrop, characterized by a remarkable lateral and vertical extent at the crest of the intrabasinal high, formed during this mature stage (Fig. 9b2). Subsequently, the structure was accreted in the prism and the seepage system deactivated. Where fold uplift is unable to keep pace with foredeep sedimentation rates and regional subsidence, coarser basin plain turbidites will onlap onto the ridge before being buried. In such a case, the pelitic interval is preserved within the arenaceous succession. The growth and the uplift of the structural high creates favorable conditions for gas-hydrate dissociation by the upward movement of the gas hydrate stability zone (e.g. Paull et al., 1994). The focusing of fluids underneath the crest of the anticline might also be favored by the shallowing of the base of gas hydrate stability zone in proximity of the main fault, due to the advection of warm fluids (Laird and Morley, 2011; Klaucke et al., 2015). The dynamics of gas hydrates could therefore be an additional controlling factor for seepage distribution on the ridge.

Seeps also developed in a more internal position on the slope of the accretionary wedge, within hemipelagites draping thrust-bounded folds that are composed of the older imbricated units. This situation is well expressed by the Moggiona outcrop. Although the temporal/structural relationships between the two systems discussed above are difficult to assess in the fossil record,, it is possible thatseeps on the wedge slope may have exploited the migration pathways of the previously deactivated foredeep seepage systems after being accreted to the prism.

7. Conclusions

Remarkable seep-related MDAC outcrops of Miocene age located within accretionary wedge-foredeep system of the northern Apennines have been characterized through geological mapping, facies analysis, and dating the host sediments by nannofossil biostratigraphy.

Our observations allow a summary of recurring features at seep carbonate outcrops in terms of their morphology, spatial distribution, lateral and vertical contacts with enclosing sediments and carbonate facies. Based on these features, we argue that seepage occurs in specific positions controlled by hosting thrust-fold structures, notably at the crest and on the forelimb, both within and external to the advancing wedge. Our findings are enriched and supported by a comparison with two modern analogues, the Hikurangi Margin, offshore New Zealand and Hydrate Ridge, on the Cascadia margin offshore Oregon, U.S.A., that share a similar compressive structural setting at the front of accretionary prisms, and are marked by widespread and thick seep-carbonate bodies. Integrating the evidence from fossil seeps and the modern analogues, we propose a new evolutionary model for seepage systems on accretionary ridges, which provides an unequivocal link between the development of fault-related anticlines and the onset and evolution of the seepage. Carbonates precipitated during different stages of the accretionary wedge migration, both in slope deposits on the frontal part of the wedge in relation to buried anticlines, and on intrabasinal ridges of the inner foredeep. During ridge growth, fluid migration pathways and seep carbonate precipitation moved from the forelimb of the structure toward its crest, following the development of extensional fractures and faults.

Acknowledgements

This work has been supported by an IAS Post-Graduate Grant 2nd session 2017 (International Association of Sedimentologists) and by the University of Modena and Reggio Emilia PhD student research grant. Special thanks to the Associate Editor Daniel Praeg, to Maciej Bojanowski and an anonymous reviewer for useful comments and suggestions that greatly improved the manuscript.

546 **References**

547 Aharon, P., Sen Gupta, B. K., 1994. Bathymetric reconstructions of the Miocene-age "calcari a
548 Lucina" (northern Apennines, Italy) from oxygen isotopes and benthic Foraminifera. Geo-Mar.
549 Lett., 14(2-3), 219-230.

550 Andresen, K. J., 2012. Fluid flow features in hydrocarbon plumbing systems: What do they tell us
551 about the basin evolution? Mar. Geol., 332, 89-108.

552 Argentino, C., Reghizzi, M., Conti, S., Fioroni, C., Fontana, D., Salocchi, A. C., 2017. Strontium
553 isotope stratigraphy as a contribution for dating Miocene shelf carbonates (S. Marino Fm, Northern
554 Apennines). Riv. It. Paleontol. Strat. 123(1), 39-59.

555 Argnani, A., Ricci Lucchi, F., 2001. Tertiary silicoclastic turbidite systems of the Northern
556 Apennines. In: Vai, F., Martini, I. P. (Eds.), Anatomy of an orogen: the Apennines and adjacent
557 Mediterranean basins. Springer, Dordrecht, 327-349.

558 Barnes, P. M., Lamarche, G., Bialas, J., Henrys, S., Pecher, I., Netzeband, G. L., Greinert, J.,
559 Mountjoy, J. J., Pedley, K., Crutchley, G., 2010. Tectonic and geological framework for gas
560 hydrates and cold seeps on the Hikurangi subduction margin, New Zealand. Mar. Geol., 272(1-4),
561 26-48.

562 Bayon, G., Henderson, G. M., Bohn, M., 2009. U-Th stratigraphy of a cold seep carbonate crust.
563 Chem. Geol., 260(1-2), 47-56.

564 Beaudoin, N., Huyghe, D., Bellahsen, N., Lacombe, O., Emmanuel, L., Mouthereau, F., Ouanhnon,
565 L., 2015. Fluid systems and fracture development during syn-depositional fold growth: An example
566 from the Pico del Aguila anticline, Sierras Exteriores, southern Pyrenees, Spain. J. Str. Geol., 70,
567 23-38.

568 Boetius, A., Wenzhöfer, F., 2013. Seafloor oxygen consumption fuelled by methane from cold
569 seeps. Nature Geosci., 6(9), p.725.

570 Bohrmann, G., Greinert, J., Suess, E., & Torres, M., 1998. Authigenic carbonates from the Cascadia
571 subduction zone and their relation to gas hydrate stability. Geology, 26(7), 647-650.

572 Bojanowski, M. J., 2007. Oligocene cold-seep carbonates from the Carpathians and their inferred
573 relation to gas hydrates. Facies, 53(3), 347-360.

574 Bojanowski, M.J., Bagiński, B., Guillermier, C., Franchi, I.A., 2015. Carbon and oxygen isotope
575 analysis of hydrate-associated Oligocene authigenic carbonates using NanoSIMS and IRMS. Chem.
576 Geol., 416, 51-64.

577 Bolton, A. J., Ben Clennell, M., Maltman, A. J., 1999. Nonlinear stress dependence of permeability:
578 A mechanism for episodic fluid flow in accretionary wedges. Geology, 27(3), 239-242.

579 Bowden, D. A., Rowden, A. A., Thurber, A. R., Baco, A. R., Levin, L. A., Smith, C. R., 2013. Cold
580 seep epifaunal communities on the Hikurangi Margin, New Zealand: composition, succession, and
581 vulnerability to human activities. PLoS One, 8(10), e76869.

582 Canfield, D. E., 1994. Factors influencing organic carbon preservation in marine sediments. Chem.
583 Geol., 114(3-4), 315-329.

584 Carminati, E., Doglioni, C., 2012. Alps vs. Apennines: the paradigm of a tectonically asymmetric
585 Earth. Earth-Sci. Rev., 112(1), 67-96.

586 Carson, B., Screaton, E. J., 1998. Fluid flow in accretionary prisms: Evidence for focused, time□
587 variable discharge. Rev. Geophys., 36(3), 329-351.

588 Chen, N.C., Yang, T.F., Hong, W.L., Chen, H.W., Chen, H.C., Hu, C.Y., Huang, Y.C., Lin, S., Lin,
589 L.H., Su, C.C., Liao, W.Z., 2017. Production, consumption, and migration of methane in
590 accretionary prism of southwestern Taiwan. Geochem. Geophys. Geosyst., 18, 2970-2989,

591 Cochonat, P., Cadet, J. P., Lallemant, S. J., Mazzotti, S., Nouzé, H., Fouchet, C., Foucher, J. P.,
592 2002. Slope instabilities and gravity processes in fuid migration and tectonically active environment
593 in the eastern Nankai accretionary wedge (KAIKO-Tokai'96 cruise). Mar. Geol., 187, 193-202.

Conti, S., Fontana, D., Gubertini, A., Sighinolfi, G., Tateo, F., Fioroni, C., Fregni, P., 2004. A multidisciplinary study of middle Miocene seep-carbonates from the northern Apennine foredeep (Italy). Sediment. Geol., 169(1-2), 1-19.

Conti S., Fontana D., Lucente C.C., 2008. Authigenic seep-carbonates cementing coarse-grained deposits in a fan-delta depositional system (middle Miocene, Marnoso-arenacea Formation, central Italy). Sedimentol. 55 (2), 471-486.

Conti S., Fontana D., Mecozzi S., Panieri G., Pini G.A., 2010. Late Miocene seep-carbonates and fluid migration on top of the Montepetra intrabasinal high (Northern Apennines, Italy): Relations with synsedimentary folding. Sediment. Geol. 231, 41-54

Conti S., Fioroni C., Fontana D., Grillenzoni C., 2016. Depositional history of the Epiligurian wedge-top basin in the Val Marecchia area (northern Apennines, Italy): a revision of the Burdigalian-Tortonian succession. Ital. J. Geosci., Vol. 135(2), 324-335.

Conti, S., Fioroni, C., Fontana, D., 2017. Correlating shelf carbonate evolutive phases with fluid expulsion episodes in the foredeep (Miocene, northern Apennines, Italy). Mar. Pet. Geol., 79, 351-359.

Crutchley, G. J., Pecher, I. A., Gorman, A. R., Henrys, S. A., Greinert, J., 2010. Seismic imaging of gas conduits beneath seafloor seep sites in a shallow marine gas hydrate province, Hikurangi Margin, New Zealand. Mar. Geol., 272(1-4), 114-126.

Crutchley, G. J., Berndt, C., Geiger, S., Klaeschen, D., Papenberg, C., Klaucke, I., Hornbach, M. J., Bangs, L. B., Maier, C., 2013. Drivers of focused fluid flow and methane seepage at south Hydrate Ridge, offshore Oregon, USA. Geology, 41(5), 551-554.

Crutchley, G. J., Fraser, D. R. A., Pecher, I. A., Gorman, A. R., Maslen, G., Henrys, S. A., 2015. Gas migration into gas hydrate□bearing sediments on the southern Hikurangi margin of New Zealand. J. Geophys. Res. Solid Earth, 120(2), 725-743.

618 Davis, E. E., Hyndman, R. D., 1989. Accretion and recent deformation of sediments along the
619 northern Cascadia subduction zone. Geol. Soc. Am. Bull., 101(11), 1465-1480.

620 Dela Pierre, F., Martire, L., Natalicchio, M., Clari, P., Petrea, C., 2010. Authigenic carbonates in
621 Upper Miocene sediments of the Tertiary Piedmont Basin (NW Italy): Vestiges of an ancient gas
622 hydrate stability zone? Geol. Soc. Am. Bull., 122(7-8), 994-1010.

623 Di Giulio, A., Mancin, N., Martelli, L., Sani, F., 2013. Foredeep palaeobathymetry and subsidence
624 trends during advancing then retreating subduction: the Northern Apennine case (Oligocene–
625 Miocene, Italy). Basin Res., 25(3), 260-284.

626 Ding, F., Spiess, V., Fekete, N., Murton, B., Brüning, M., Bohrmann, G., 2010. Interaction between
627 accretionary thrust faulting and slope sedimentation at the frontal Makran accretionary prism and its
628 implications for hydrocarbon fluid seepage. J. Geophys. Res. Solid Earth, 115(B8).

629 Dumke, I., Klaucke, I., Berndt, C., Bialas, J., 2014. Sidescan backscatter variations of cold seeps on
630 the Hikurangi Margin (New Zealand): indications for different stages in seep development. Geo-
631 Mar. Lett., 34(2-3), 169-184.

632 Ellis, S., Pecher, I., Kukowski, N., Xu, W., Henrys, S., Greinert, J., 2010. Testing proposed
633 mechanisms for seafloor weakening at the top of gas hydrate stability on an uplifted submarine
634 ridge (Rock Garden), New Zealand. Mar. Geol., 272(1), 127-140.

635 Evans, M. A., Fischer, M. P., 2012. On the distribution of fluids in folds: A review of controlling
636 factors and processes. J. Str. Geol., 44, 2-24.

637 Fontana, D., Conti, S., Grillenzoni, C., Mecozzi, S., Petrucci, F., Turco, E., 2013. Evidence of
638 climatic control on hydrocarbon seepage in the Miocene of the northern Apennines: the case study
639 of the Vicchio Marls. Mar. Pet. Geol., 48, 90-99.

640 Fraser, D. R., Gorman, A. R., Pecher, I. A., Crutchley, G. J., Henrys, S. A., 2016. Gas hydrate
641 accumulations related to focused fluid flow in the Pegasus Basin, southern Hikurangi Margin, New
642 Zealand. Mar. Pet. Geol., 77, 399-408.

643 Gill, F. L., Harding, I. C., Little, C. T., Todd, J. A., 2005. Palaeogene and Neogene cold seep
644 communities in Barbados, Trinidad and Venezuela: An overview. Palaeogeogr. Palaeoclimatol.
645 Palaeoecol., 227(1), 191-209.

646 Goldfinger, C., Kulm, L.D., Yeats, R.S., McNeill, L., & Hummon, C., 1997. Oblique strike-slip
647 faulting of the central Cascadia submarine forearc. J. Geophys. Res., 102(B4):8217-8244.

648 Goldfinger, C., Yeats, R.S., Kulm, L.D., Applegate, B., MacKay, M.E., Moore, G.F., 1992.
649 Transverse structural trends along the Oregon convergent margin: implications for Cascadia
650 earthquake potential and crustal rotations. Geology, 20, 141-144.

651 Greinert, J., Bohrmann, G., Suess, E., 2001. Gas hydrate-associated carbonates and methane-
652 venting at Hydrate Ridge: classification, distribution and origin of authigenic lithologies. In Paul,
653 C.K., and Dillon, W.P. (Eds.), Natural Gas Hydrates: Occurrence, Distribution, and
654 Detection. Geophys. Monogr., 124:99-114.

655 Greinert, J., Lewis, K. B., Bialas, J., Pecher, I. A., Rowden, A., Bowden, D.A., De Batist, M. A.,
656 Linke, P., 2010. Methane seepage along the Hikurangi Margin, New Zealand: Overview of studies
657 in 2006 and 2007 and new evidence from visual, bathymetric and hydroacoustic
658 investigations. Mar. Geol., 272(1), 6-25.

659 Grillenzoni, C., Monegatti, P., Turco, E., Conti, S., Fioroni, C., Fontana, D., Salocchi, A. C., 2017.
660 Paleoenvironmental evolution in a high-stressed cold-seep system (Vicchio Marls, Miocene,
661 northern Apennines, Italy). Palaeogeogr. Palaeoclimatol. Palaeoecol., 487, 37-50.

662 Ho, S., Cartwright, J. A., Imbert, P., 2012. Vertical evolution of fluid venting structures in relation
663 to gas flux, in the Neogene-Quaternary of the Lower Congo Basin, Offshore Angola. Mar.
664 Geol., 332, 40-55.

665 Hovland, M., 2002. On the self-sealing nature of marine seeps. Cont. Shelf Res., 22(16), 2387-
666 2394.

667 Johnson, J. E., Goldfinger, C., Suess, E., 2003. Geophysical constraints on the surface distribution
668 of authigenic carbonates across the Hydrate Ridge region, Cascadia margin. Mar. Geol., 202(1), 79-
669 120.

670 Johnson, J. E., Goldfinger, C., Tréhu, A. M., Bangs, N. L. B., Torres, M. E., Chevallier, J., 2006.
671 North-south variability in the history of deformation and fluid venting across Hydrate Ridge,
672 Cascadia margin. Proc. ODP, Sci. Results, 199.

673 Jones, A. T., Greinert, J., Bowden, D. A., Klaucke, I., Petersen, C. J., Netzeband, G. L., Weinrebe,
674 W., 2010. Acoustic and visual characterisation of methane-rich seabed seeps at Omakere Ridge on
675 the Hikurangi Margin, New Zealand. Mar. Geol., 272(1-4), 154-169.

676 Jørgensen, B., 1982. Mineralization of organic matter in the sea bed - the role of sulfate reduction.
677 Nature 296, 643-645

678 Judd, A., Hovland, M., 2009. Seabed fluid flow: the impact on geology, biology and the marine
679 environment. Cambridge University Press.

680 Kiel, S., Tyler, P.A., 2010. Chemosynthetically-driven ecosystems in the Deep Sea. In: Kiel, S.
681 (Ed.), The Vent and Seep Biota. Springer, Dordrecht, 1-14.

682 Klaucke, I., Weinrebe, W., Petersen, C. J., Bowden, D., 2010. Temporal variability of gas seeps
683 offshore New Zealand: Multi-frequency geoacoustic imaging of the Wairarapa area, Hikurangi
684 margin. Mar. Geol., 272(1-4), 49-58.

685 Klaucke, I., Berndt, C., Crutchley, G., Chi, W. C., Lin, S., Muff, S., 2015. Fluid venting and
686 seepage at accretionary ridges: the Four Way Closure Ridge offshore SW Taiwan. Geo-Mar.
687 Lett., 36(3), 165-174.

688 Koch, S., Berndt, C., Bialas, J., Haeckel, M., Crutchley, G., Papenberg, C., Klaeschen, D., Greinert,
689 J., 2015. Gas-controlled seafloor doming. Geology, 43(7), 571-574.

690 Koch, S., Schroeder, H., Haeckel, M., Berndt, C., Bialas, J., Papenberg, C., Klaeschen, D., Plaza-
691 Faverola, A., 2016. Gas migration through Opouawe Bank at the Hikurangi margin offshore New
692 Zealand. Geo-Mar. Lett., 36(3), 187-196.

693 Krabbenhoeft, A., Bialas, J., Klaucke, I., Crutchley, G., Papenberg, C., Netzeband, G. L., 2013.
694 Patterns of subsurface fluid-flow at cold seeps: The Hikurangi Margin, offshore New Zealand. Mar.
695 Pet. Geol., 39(1), 59-73.

696 Laird, A. P., Morley, C. K., 2011. Development of gas hydrates in a deep-water anticline based on
697 attribute analysis from three-dimensional seismic data. Geosphere, 7(1), 240-259.

698 Leifer, I., Kamerling, M. J., Luyendyk, B. P., Wilson, D. S., 2010. Geologic control of natural
699 marine hydrocarbon seep emissions, Coal Oil Point seep field, California. Geo-Mar. Lett., 30(3-4),
700 331-338.

701 Liebetrau, V., Eisenhauer, A., Linke, P., 2010. Cold seep carbonates and associated cold-water
702 corals at the Hikurangi Margin, New Zealand: new insights into fluid pathways, growth structures
703 and geochronology. Mar. Geol., 272(1-4), 307-318.

704 Luff, R., Wallmann, K., 2003. Fluid flow, methane fluxes, carbonate precipitation and
705 biogeochemical turnover in gas hydrate-bearing sediments at Hydrate Ridge, Cascadia Margin:
706 numerical modeling and mass balances. Geochim. Cosmochim. Acta, 67(18), 3403-3421.

707 MacKay, M.E., Moore, G.F., Cochrane, G.R., Moore, J.C., Kulm, L.D., 1992. Landward vergence
708 and oblique structural trends in the Oregon margin accretionary prism: implications and effect on
709 fluid flow. Earth Planet. Sci. Lett., 109:477-491.

710 Mohammedyasin, S. M., Lippard, S. J., Omosanya, K. O., Johansen, S. E., Harishidayat, D., 2016.
711 Deep-seated faults and hydrocarbon leakage in the Snøhvit Gas Field, Hammerfest Basin,
712 Southwestern Barents Sea. Mar. Pet. Geol., 77, 160-178.

713 Moore, J. C., Orange, D., Kulm, L. D., 1990. Interrelationship of fluid venting and structural
714 evolution: Alvin observations from the frontal accretionary prism, Oregon. J. Geophys. Res. Solid
715 Earth, 95(B6), 8795-8808.

716 Moretti, I., Labaume, P., Sheppard, S. M., Boulègue, J., 2002. Compartmentalisation of fluid
717 migration pathways in the sub-Andean Zone, Bolivia. Tectonophysics, 348(1), 5-24.

718 Morley, C. K., 2007. Development of crestal normal faults associated with deepwater fold
719 growth. J. Str. Geol., 29(7), 1148-1163.

720 Morley, C. K., Warren, J., Tingay, M., Boonyasaknanon, P., Julapour, A., 2014. Reprint of:
721 Comparison of modern fluid distribution, pressure and flow in sediments associated with anticlines
722 growing in deepwater (Brunei) and continental environments (Iran). Mar. Pet. Geol., 55, 230-249.

723 Nelson, C. S., Nyman, S. L., Campbell, K. A., Rowland, J. R., 2017. Influence of faulting on the
724 distribution and development of cold seep-related dolomitic conduit concretions at East Cape, New
725 Zealand. N.Z. J. Geol. Geophys., 60 (4), 487-496.

726 Netzeband, G. L., Krabbenhöft, A., Zillmer, M., Petersen, C. J., Papenberg, C., Bialas, J., 2010. The
727 structures beneath submarine methane seeps: seismic evidence from Opouawe Bank, Hikurangi
728 Margin, New Zealand. Mar. Geol., 272(1), 59-70.

729 Nyman, S. L., Nelson, C. S., Campbell, K. A., 2010. Miocene tubular concretions in East Coast
730 Basin, New Zealand: analogue for the subsurface plumbing of cold seeps. Mar. Geol. 272 (1-4),
731 319-336.

732 Paull, C. K., Ussle, W., Borowski, W. S., 1994, Sources of Biogenic Methane to Form Marine Gas
733 Hydrates In Situ Production or Upward Migration? Ann. N.Y. Acad. Sci., 715(1), 392-409.

734 Pierre, C., Rouchy, J. M., 2004. Isotopic compositions of diagenetic dolomites in the Tortonian
735 marls of the western Mediterranean margins: evidence of past gas hydrate formation and
736 dissociation. Chem. Geol., 205(3-4), 469-484.

737 Plaza-Faverola, A., Bünz, S., Mienert, J., 2011. Repeated fluid expulsion through sub-seabed
738 chimneys offshore Norway in response to glacial cycles. Earth Planet. Sci. Lett., 305(3), 297-308.

739 Plaza□Faverola, A., Henrys, S., Pecher, I., Wallace, L., Klaeschen, D., 2016. Splay fault branching
740 from the Hikurangi subduction shear zone: Implications for slow slip and fluid flow. Geochem.
741 Geophys. Geosyst., 17(12), 5009-5023.

742 Riedel, M., Crutchley, G., Koch, S., Berndt, C., Bialas, J., Eisenberg-Klein, G., Prüßmann, J.,
743 Papenberg, C., Klaeschen, D., 2018. Elongate fluid flow structures: Stress control on gas migration
744 at Opouawe Bank, New Zealand. Mar. Pet. Geol., 92, 913-931

745 Sibson, R. H. (2000). Fluid involvement in normal faulting. J. Geodyn., 29(3-5), 469-499.

746 Suess, E., Torres, M. E., Bohrmann, G., Collier, R. W., Greinert, J., Linke, P., Rehder, G., Tréhu,
747 A., Wallmann, K., Winckler, G., Zuleger, E., 1999. Gas hydrate destabilization: enhanced
748 dewatering, benthic material turnover and large methane plumes at the Cascadia convergent margin.
749 Earth Planet. Sci. Lett. 170:1-15

750 Tavani, S., Storti, F., Lacombe, O., Corradetti, A., Muñoz, J. A., Mazzoli, S., 2015. A review of
751 deformation pattern templates in foreland basin systems and fold-and-thrust belts: Implications for
752 the state of stress in the frontal regions of thrust wedges. Earth-Sci. Rev., 141, 82-104.

753 Taviani, M., 2014. Marine chemosynthesis in the Mediterranean Sea. In: Goffredo, S., Dubinsky Z.
754 (Eds.), The Mediterranean Sea. Springer, Dordrecht, 69-83.

755 Teichert, B. M. A., Eisenhauer, A., Bohrmann, G., Haase-Schramm, A., Bock, B., & Linke, P.
756 (2003). U/Th systematics and ages of authigenic carbonates from Hydrate Ridge, Cascadia Margin:
757 recorders of fluid flow variations. Geochim. Cosmochim. Acta, 67(20), 3845-3857.

758 Teichert, B. M. A., Johnson, J. E., Solomon, E. A., Giosan, L., Rose, K., Kocherla, M., Connolly,
759 E.C., Torres, M.E., 2014. Composition and origin of authigenic carbonates in the Krishna-Godavari
760 and Mahanadi Basins, eastern continental margin of India. Mar. Pet. Geol. 58, 438-460

761 Tinterri, R., Muzzi-Magalhaes, P., 2011. Synsedimentary structural control on foredeep turbidites:
762 an example from Miocene Marnoso-arenacea Formation, Northern Apennines, Italy. Mar. Pet.
763 Geol., 28(3), 629-657.

764 Torres, M.E., Wallmann, K., Tréhu, A.M., Bohrmann, G., Borowski, W.S., Tomaru, H., 2004. Gas
765 hydrate growth, methane transport, and chloride enrichment at the southern summit of Hydrate
766 Ridge, Cascadia margin off Oregon. Earth Planet. Sci. Lett., 226(1-2):225-241

767 Townend, J., 1997. Subducting a sponge: minimum estimates of the fluid budget of the Hikurangi
768 Margin accretionary prism. Geological Society of New Zealand Newsletter, 112, 14-16.

769 Trehu, A. M., Torres, M. E., Moore, G. F., Suess, E., Bohrmann, G., 1999. Temporal and spatial
770 evolution of a gas hydrate-bearing accretionary ridge on the Oregon continental
771 margin. Geology, 27(10), 939-942

772 Trehu, A.M., Long, P.E., Torres, M.E., Bohrmann, G.R.R.F., Rack, F.R., Collett, T.S., Goldberg,
773 D.S., Milkov, A.V., Riedel, M., Schultheiss, P., Bangs, N.L., 2004. Three-dimensional distribution
774 of gas hydrate beneath southern Hydrate Ridge: constraints from ODP Leg 204. Earth Planet. Sci.
775 Lett., 222(3), 845-862.

776 Tryon, M. D., Brown, K. M., 2001. Complex flow patterns through Hydrate Ridge and their impact
777 on seep biota. Geophys. Res. Lett., 28(14), 2863-2866.

778 Weinberger, J.L., Brown, K.M., Long, P.E., 2005. Painting a picture of gas hydrate distribution
779 with thermal images. Geophys. Res. Lett., 32(4):L04609.

780 Whiticar, M. J. (1999). Carbon and hydrogen isotope systematics of bacterial formation and
781 oxidation of methane. Chem. Geol., 161(1-3), 291-314.

782 Yamada, Y., Baba, K., Miyakawa, A., Matsuoka, T., 2014. Granular experiments of thrust wedges:
783 insights relevant to methane hydrate exploration at the Nankai accretionary prism. Mar. Pet. Geol.,
784 51, 34-48.

785
786

787 **Figure captions**

788 Fig. 1.Simplified geological map of the northern Apennines (Italy) showing the main structural
789 units and the location of the studied outcrops: MOG, CA and COR and stand for Moggiona,
790 Castagno d'Andrea and Corella, respectively.

791 Fig. 2. Diagram showing the main structural elements of the Apennine wedge-foredeep system
792 during the Miocene and their relationships with underlying structures. The structural position of
793 seeps discussed in this study is also indicated. A. Seeps on the slope of the accretionary wedge,
794 associated with buried anticlinal ridges covered by a hemipelagic slope deposits (Moggiona). B.
795 Seeps on intrabasinal highs at the deformation front (Castagno d'Andrea and Corella). Not to scale.

796 Fig. 3. Geological maps and cross sections of the studied outcrops displaying the spatial distribution
797 of seep-carbonates (in red) and their relationships with regional thrusts and the main structural trend
798 (NW-SE). a) Moggiona b) Castagno d'Andrea c) Corella. Authigenic carbonate bodies are
799 concordant to bedding and are always located in proximity of and parallel to major overthrusts.

800 Fig. 4. Calcareous nannofossil biostratigraphic scheme for the Lower-Middle Miocene of the
801 Mediterranean area showing the chronostratigraphic position of the studied outcrops (MOG, CA,
802 COR). FCO= first common occurrence; LCO= last common occurrence; LO= last occurrence; PB=
803 paracme beginning; PE= paracme end; AS= acme spike.

804 Fig. 5. Examples of carbonate geometries and relationships with the host sediments at the
805 Moggiona outcrop: a) Plan view of the MDACs (in red) showing their spatial distribution and
806 dimensions. Carbonate bodies are concordant with subvertical host strata, hence the widths at

807 outcrop approximate their thicknesses. The circular dashed line indicates the area shown in c. b)
808 facies distribution on the largest (~100 m wide) carbonate body. c) Close up view of minor satellite
809 blocks and bifurcating lateral termination from the same body of b. Authigenic carbonates are
810 highlighted in pink on the right side of the figure.

811 Fig. 6. Examples of recurring carbonate facies in the examined seep sites. a) Conduits at the base of
812 a carbonate body at the Moggiona outcrop. They are few meters long, up to 2 cm in diameter (close
813 up at bottom right) and are oriented perpendicular to the basal surface of the body. b) Autoclastic
814 breccias in seep-carbonates, Castagno d'Andrea outcrop. c) Carbonate-filled fractures at Corella
815 outcrop. d) Densely packed chemosynthetic fauna (Lucinid clams), Corella outcrop.

816 Fig. 7. Examples of different carbonate geometries and relationships with the host sediments at the
817 Castagno d'Andrea outcrop. a) The main carbonate body shows an irregular profile with strong
818 lateral thickness variations and a bifurcated termination. b) Pinnacle-like structures marked by an
819 irregular lateral geometry that results in a christmas-tree like profile. c) Facies distribution of the
820 same body. d) Small carbonate concretions occurring at the base of a pinnacular body.

821 Fig. 8. Carbonate geometries and relationships with the host sediments at the Corella outcrop. a)
822 Distributions and shape of seep-carbonates as mapped in Figure 3c; the carbonate bodies (in red)
823 are concordant with subvertical host strata, so their widths at outcrop correspond to thicknesses. b)
824 Facies mapping within the carbonate body represented in the left side, showing the distribution of
825 conduit-rich facies and seep-related fauna. The circular dashed line indicates the area shown in c. c)
826 Vertically stacked lenticular carbonate bodies alternated with small concretions showing
827 relationships with hosting sediments.

828 Fig. 9. Conceptual models of development of seeps above thrust-related anticlines in two different
829 structural positions in the wedge-foredeep system. a) on the slope of the accretionary wedge on
830 hemipelagic sediments draping buried anticlines; active thrust and extensional faults in the anticline
831 are the main fluid migration pathways and sustain seepage at the seafloor (the Moggiona outcrop is

832 well representative of this type of seepage). b) within the foredeep basin at the leading edge of the
833 deformation front; the anticline acts as an intrabasinal high segmenting the foredeep; sedimentation
834 on the anticline consists of diluted turbidites and hemipelagites. Seeps are distributed along the
835 seafloor projection of the thrust (b1). The proceeding of folding generates extensional stresses in the
836 hinge zone of the anticline, promoting the development of normal faults. During this stage, seepage
837 shifts toward the crest of the ridge following the new migration pathways (b2). Shown in yellow
838 and light blue color are terrigenous turbidites and hemipelagites respectively.

839 Tab. 1. Carbonate mineralogy and C and O isotopic composition of the studied methane-derived
840 carbonate deposits. Chemosynthetic fauna is also reported. LMC = low-Mg calcite, HMC = high-
841 Mg calcite, Dol = dolomite.

842

843 Tab. 2. Summary of main recurrent features in the three selected outcrops, representative of
844 Miocene seeps of the northern Apennines linked to thrust-related anticlines.

845

Outcrop	Carbonate component	Carbonate mineralogy	$\delta^{13}C$ (‰ VPDB)	$\delta^{18}O$ (‰ VPDB)	Chemosynthetic fauna	Reference
Corella	micrite matrix	LMC, Dol	-42.3 to -26.7	-1.5 to 1.1	Lucinid and Vesycomid clams	Argentino et al., 2017
	calcite cement	LMC	-29.5 to-26.6	-5.7 to -1.0		
Castagno d'Andrea	micrite matrix	LMC, Dol	-41.3 to -15.8	-0.9 to 1.2	Lucinid clams	Conti et al., 2004, 2017
Moggiona	micrite matrix	LMC	-40.2 to -24.9	-5.8 to 0.7	Lucinid clams	Conti et al., 2017
	calcite cement	LMC	-25.7 to -13.6	-9.9 to -1.6		

Carbonate geometries and spatial distribution		- Few isolated large (up to 250 m) stratiform bodies with constant thickness (up to 30 m), concordant to bedding of enclosing sediments (Fig. 8a) - Lenticular bodies (up to 100 m), irregular in thickness (along strike variations) (Fig. 5a, 7b) - Pinnacle-like geometry (up to 8 m high) discordant with the host sediments (Fig. 7c, d) - Composite, pinnacular to lenticular geometries, with a christmas-tree like shape (Fig 7c) - Large bodies surrounded by satellite small meter-size blocks (Fig. 7d) - Scattered meter-size bodies horizontally and vertically distributed (5a)
Relationships with the host sediments	Lateral contacts	- Pinch-out with progressive thinning of the body in few meters (Fig. 8b) - Bifurcations with large single bodies splitted in two minor branches (Fig. 5a, b; 8a) - Multiple interfingering of carbonates with host pelites (Fig. 7b, c) In each of these cases, the contact between authigenic carbonates and enclosing pelites can be sharp, due to the lithological contrast (Fig. 7a), or transitional with a progressive decrease in cementation up to scarcely cemented marls and siltstones
	Vertical contacts	- Lower and upper stratigraphic contacts between carbonates and pelitic sediments marked by sharp boundaries without connections with other bodies -Vertical repetition of highly cemented levels or concretions above major bodies, in correspondence of more permeable silty turbiditic strata - Cross-cutting relationships with vertical or subvertical protrusions and pinnacles (Fig. 3b; 7c)
Main carbonate facies		- Abundant conduits and irregular framework of veins and drusy-like cavities, associated with breccias (Fig. 6a, b). No articulated fauna; coquina debris and disarticulated shells may occur. This facies characterizes the basal portion of bodies - Polygenic and monogenic breccias, mainly in pinnacles (Fig. 6b) - Abundant articulated chemosynthetic fauna (Lucinid and Vesycomid), often in life position, mainly present in stratiform and lenticular bodies (Fig. 6d)

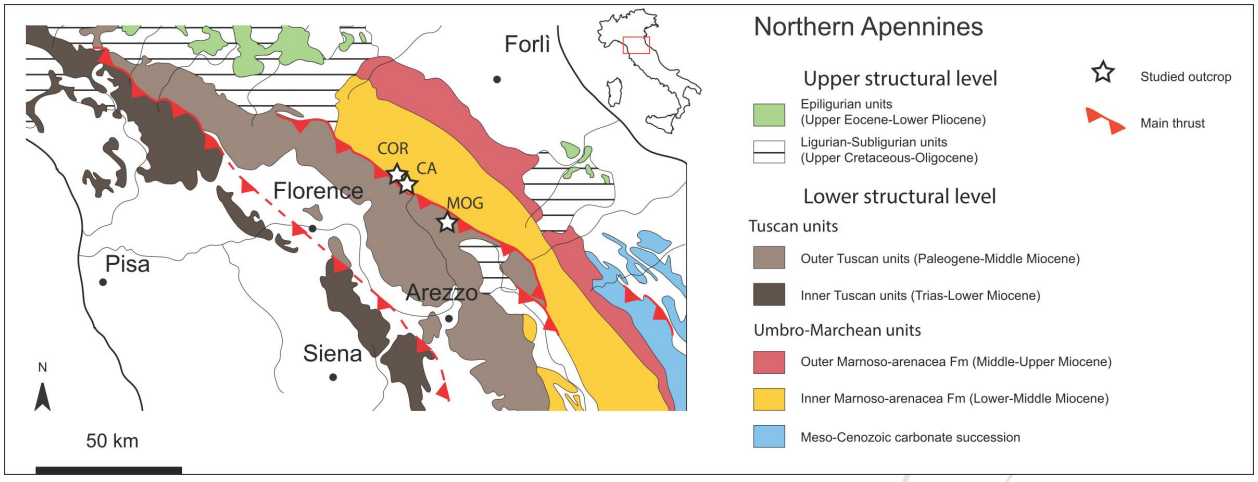

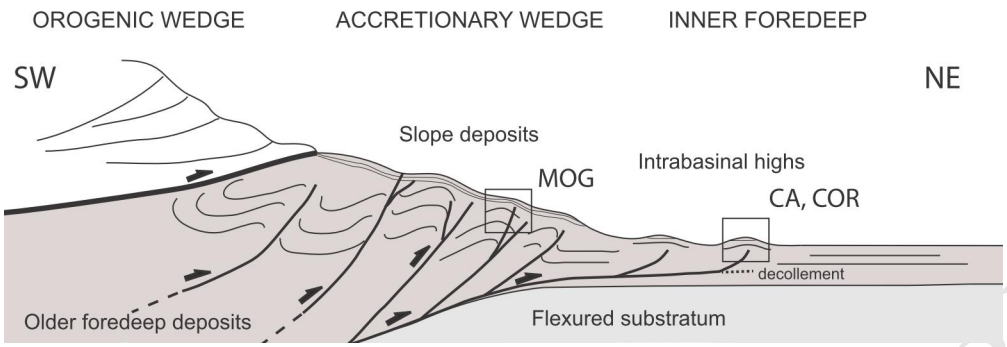

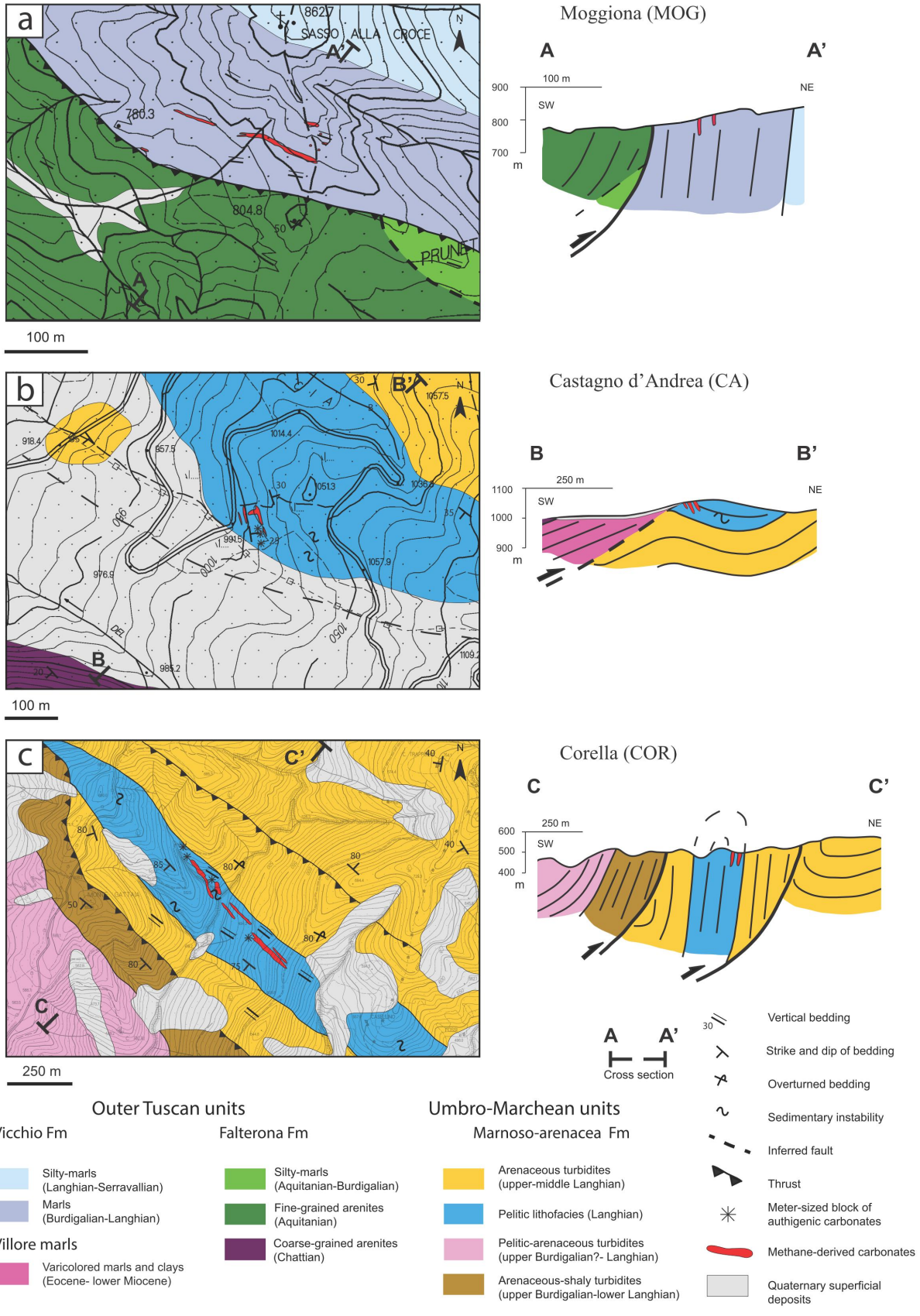
a
862.7
SASSO ALLA CROCE
A'
N
780.3
804.8
50
PRUNE
A
100 m
Moggiona (MOG)
A
A'
100 m
900
800
700
m
SW
NE
b
B'
N
1057.5
1014.4
918.4
857.5
1051.3
1036.8
991.5
1057.9
976.9
1050
985.2
B
100 m
Castagno d'Andrea (CA)
B
B'
250 m
1100
1000
900
m
SW
NE
c
C'
N
C
250 m
Corella (COR)
C
C'
600
500
400
m
SW
NE
A
A'
Cross section
Outer Tuscan units
Vicchio Fm
Silty-marls (Langhian-Serravallian)
Marls (Burdigalian-Langhian)
Villore marls
Varicolored marls and clays (Eocene- lower Miocene)
Falterona Fm
Silty-marls (Aquitanian-Burdigalian)
Fine-grained arenites (Aquitanian)
Coarse-grained arenites (Chattian)
Umbro-Marchean units
Marnoso-arenacea Fm
Arenaceous turbidites (upper-middle Langhian)
Pelitic lithofacies (Langhian)
Pelitic-arenaceous turbidites (upper Burdigalian?- Langhian)
Arenaceous-shaly turbidites (upper Burdigalian-lower Langhian)
Vertical bedding
Strike and dip of bedding
Overturned bedding
Sedimentary instability
Inferred fault
Thrust
Meter-sized block of authigenic carbonates
Methane-derived carbonates
Quaternary superficial deposits

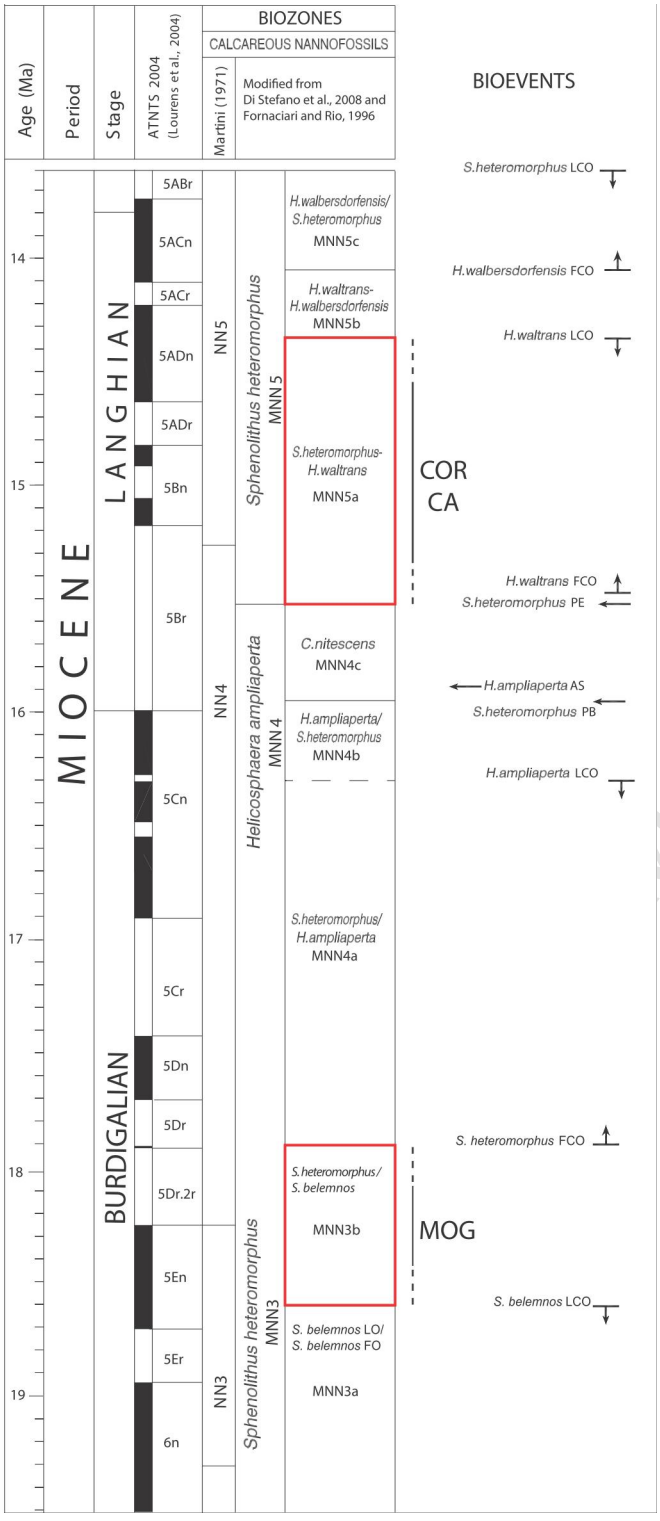

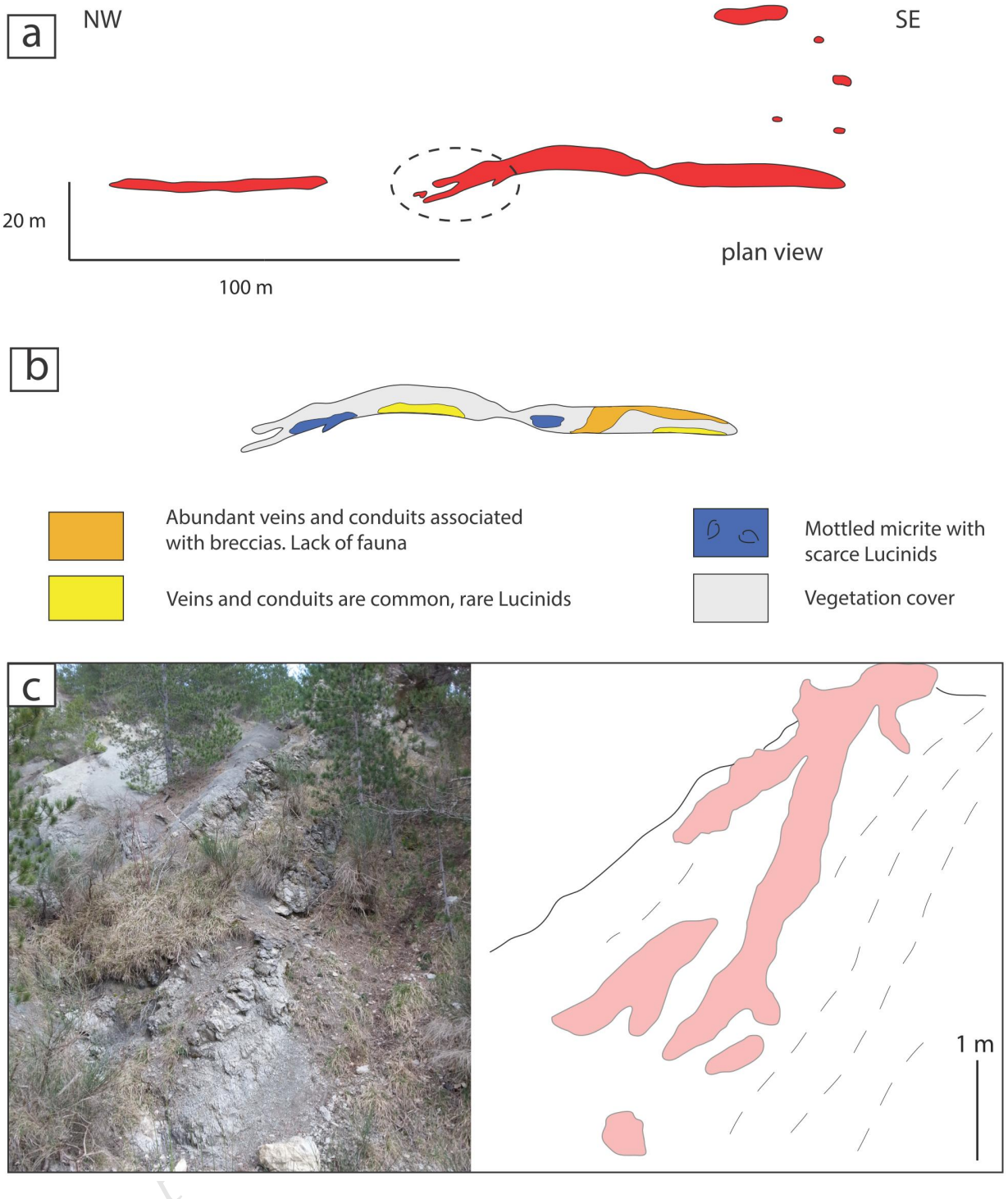
a
NW
SE
20 m
100 m
plan view
b
Abundant veins and conduits associated with breccias. Lack of fauna
Veins and conduits are common, rare Lucinids
Mottled micrite with scarce Lucinids
Vegetation cover
c
1 m

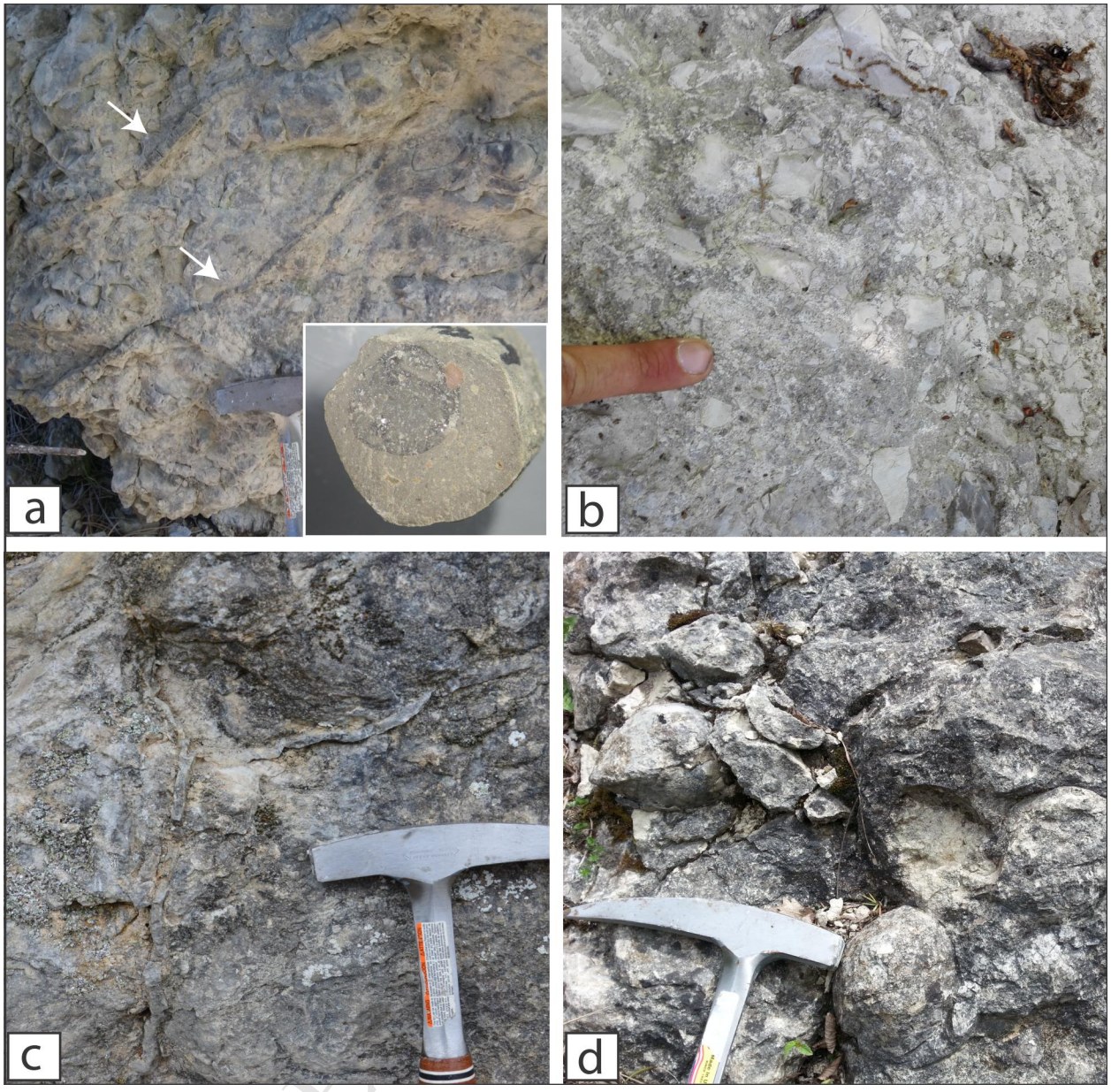

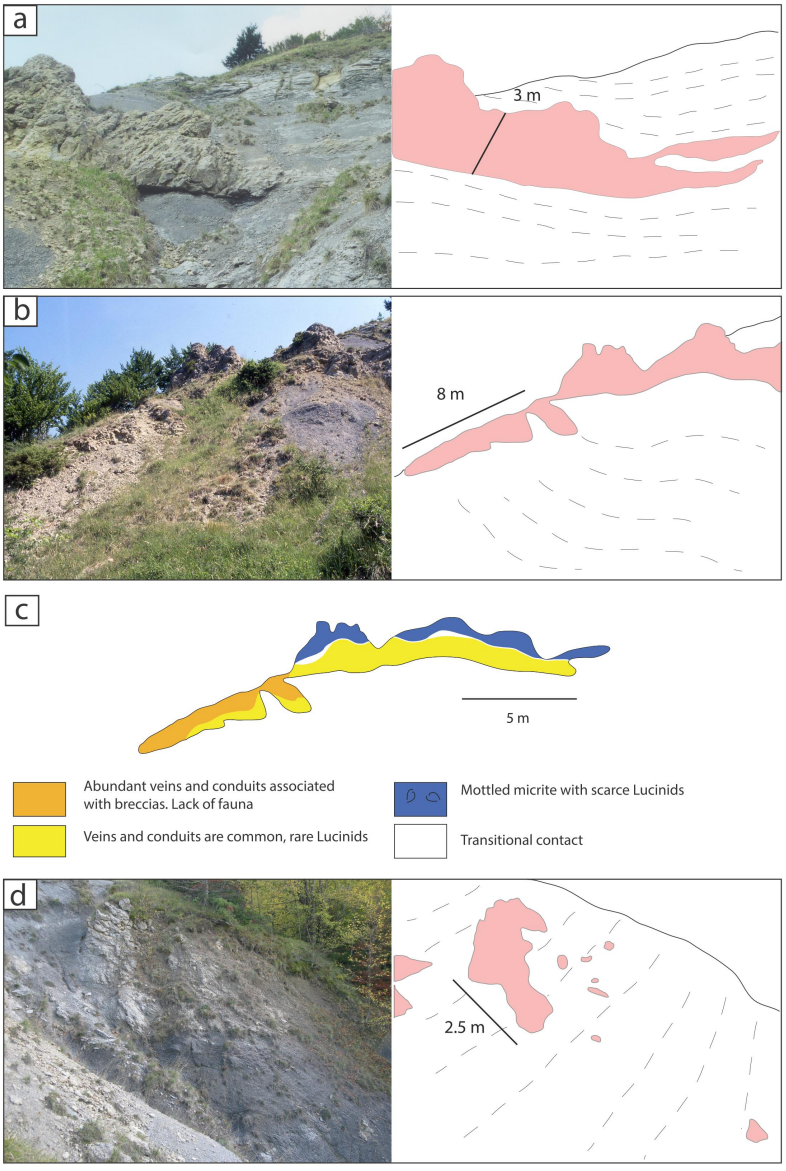

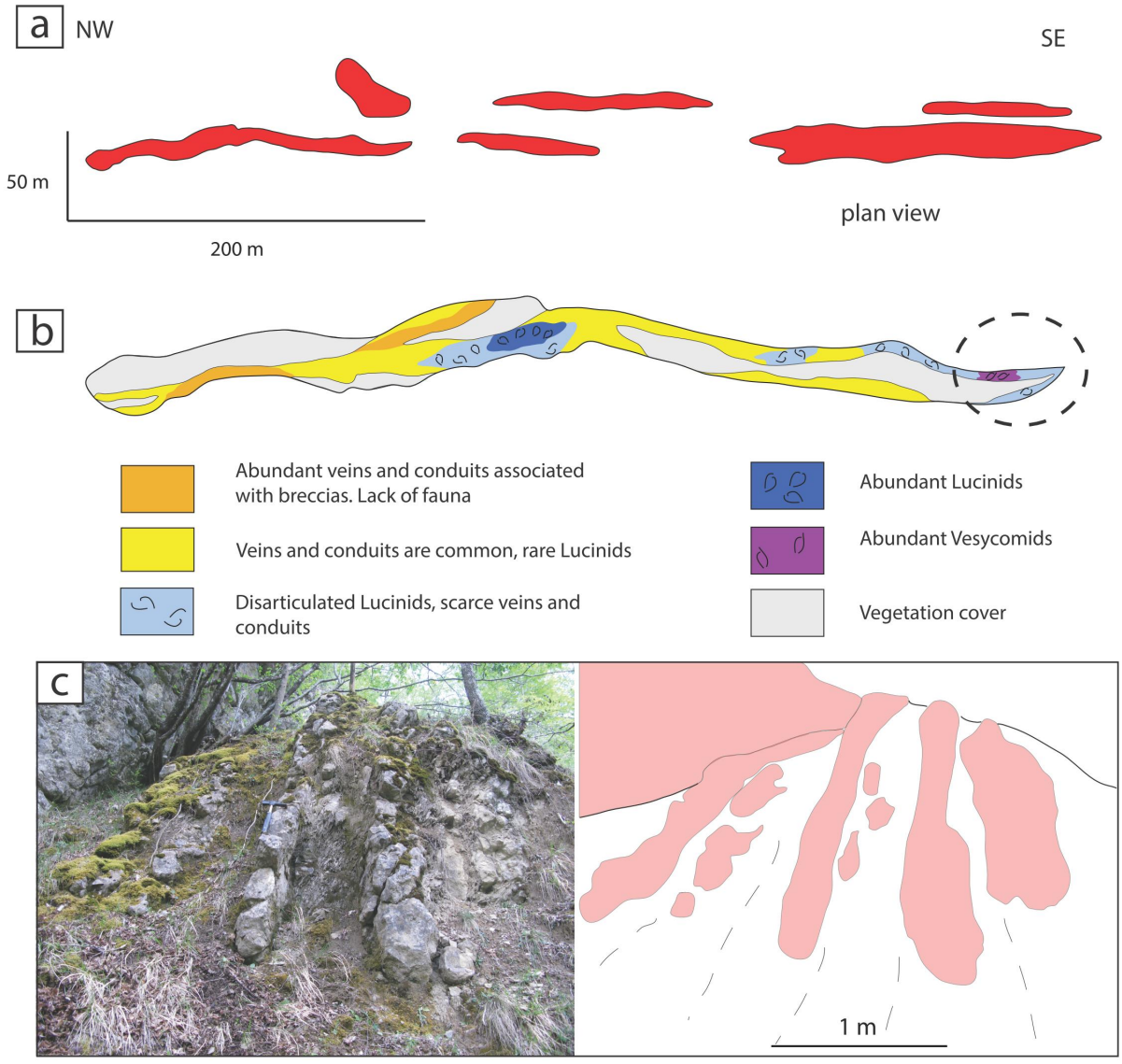
a
NW
SE
50 m
200 m
plan view
b
Abundant veins and conduits associated with breccias. Lack of fauna
Veins and conduits are common, rare Lucinids
Disarticulated Lucinids, scarce veins and conduits
Abundant Lucinids
Abundant Vesycomids
Vegetation cover
c
1 m

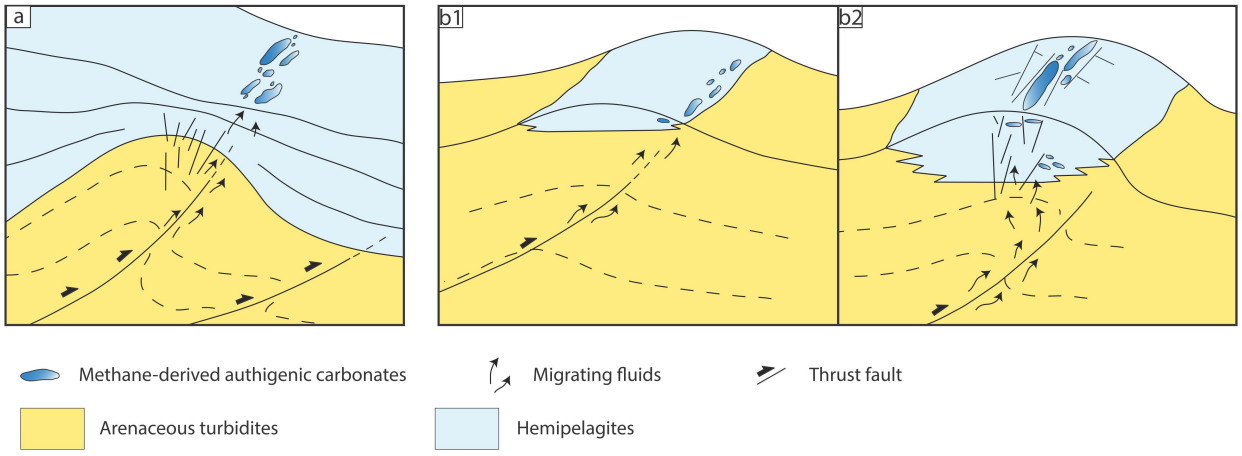

- We provide summary of recurring features at seep outcrops in the northern Apennines
- Fossil seeps are compared with analogues from modern compressive settings
- The onset and evolution of seeps are linked to the development of anticlinal ridges
- We propose a new evolutionary model for seeps on accretionary ridges